

MFEUsLNet: Skin cancer detection and classification using integrated AI with multilevel feature extraction-based unsupervised learning

Vasuja Devi Midasala^a, B. Prabhakar^b, J. Krishna Chaitanya^c, Kalyanapu Sirnivas^d, D. Eshwar^e, Pala Mahesh Kumar^{f,*}

^a Department of CSE, Mangalayatan University-Jabalpur, Jabalpur, Madhya Pradesh, India

^b Department of Electronics and Communication Engineering, JNTU College of Engineering Jagtial, Telangana, India

^c Department of Electronics and Communication Engineering, Vardhaman Engineering College, Hyderabad, Telangana, India

^d Department of Artificial Intelligence and Data Science, Seshadri Rao Gudlavalleru Engineering College, Gudlavalleru, Andhra Pradesh, India

^e Department of Computer Science and Engineering, Kommuri Pratap Reddy Institute of Technology, Hyderabad, Telangana, India

^f AI Engineer, SAK INFORMATICS, Hyderabad 500090, Telangana, India



ARTICLE INFO

Keywords:

Skin cancer detection and classification
K-means clustering
Redundant discrete wavelet transform
Gray level co-occurrence matrix
Recurrent neural networks

ABSTRACT

Skin Cancer is the most common form of the disease and is responsible for millions of deaths each year. Most of the relevant studies concentrate on algorithms that are based on machine learning, and few on deep learning as well. However, due to the several challenges in dermoscopic image acquisition, these algorithms are unable to deliver the highest possible level of accuracy and specificity. Therefore, this article implements skin cancer detection and classification (SCDC) system using multilevel feature extraction (MFE)-based artificial intelligence (AI) with unsupervised learning (USL), here after denoted as MFEUsLNet. Initially, the given skin images are preprocessed using bilateral filter, which removes the noise artifacts from the source images. Then, a well-known USL approach named K-means clustering (KMC) is used for segmentation of skin lesion, which can detect the affected skin lesion quite efficiently. Then, gray level co-occurrence matrix (GLCM), and redundant discrete wavelet transform (RDWT) are used for low level, texture and colour feature extraction. Finally, recurrent neural network (RNN) classifier is used to train with these multi-level features and classify the multiple types of skin cancer. The simulations proven that the proposed MFEUsLNet model is outperformed state-of-the-art SCDC approaches in terms of medical statistical quality metrics such as classification accuracy, specificity, precision, recall, F1-score, and sensitivity for ISIC-2020 dataset.

1. Introduction

At the current time, disorders associated with cancer are among the deadliest sorts of illnesses that endanger human life [1]. Melanoma skin cancer is one of the most serious types of cancer, and it is fatal if it is not detected and treated in its early stages. The earlier melanoma skin cancer is detected and treated, the lower the risk of death from the disease and the fewer problems that arise throughout the treatment process [2]. The procedure for making a diagnosis begins with the collection of a biopsy sample from the patient, which a dermatologist then analyzes. The outcome of the examination is contingent on the practitioner's level of expertise as well as the instruments that were used [3]. Nowadays, skin cancer is the sort of cancer that affects the most people out of all the other kinds of cancer [4], and it is either benign or

malignant. Of all these kinds, malignant skin cancer is the more dangerous of the two when compared to non-malignant skin cancer [5]. Inspection of malignant lesions requires dermatologists with much expertise. These individuals use a computer-assisted approach for the early diagnosis of malignant conditions [6]. In the process of diagnosing skin cancer, deeper learning models and their accompanying algorithms were used more. The existing classifiers and models need to be improved so that they do not suffer from the shortcomings of traditional models.

Numerous studies [7] have made use of image preprocessing to identify malignant tumours at earlier stages, which ultimately results in more successful therapy. Skilled dermatologists have established asymmetry, border, colour, diameter, and edge (ABCDE) [8,9] as standardized descriptions to aid in visualizing typical aspects of severe malignant cases. These descriptions include asymmetrical form, border

* Corresponding author.

E-mail addresses: bprabhakar@jntuh.ac.in (B. Prabhakar), kalyanapusrinivas@gecgudlavalleru.ac.in (K. Sirnivas), mahesh@sakininformatics.com (P.M. Kumar).

abnormalities, colour, diameter, and evolution. The enormous amounts of variations across the various skin tones that come from persons of diverse ethnic origins are one of the most significant obstacles when attempting to categorize serious skin injuries. Recent advances in the development of deep learning convolutional neural networks (CNN) [10,11] have made it possible for computers to outperform dermatologists in the categorization of skin cancer. The dataset plays a major role in the SCDC systems, which are used for system training.

There are different types of datasets available, such as BCN_20000 [12], HAM10000 [13], and International Skin Imaging Collaboration (ISIC) [14]. The ISIC organization has been conducting the SCDC-based

challenges since 2016 and has released the ISIC-2016, ISIC-2017, ISIC-2018, ISIC-2019, and ISIC-2020 datasets. Here, ISIC-2020 [15] is the recent challenge dataset, which contains multiple skin cancer images. The choice to primarily focus on the ISIC 2020 dataset in this study was driven by its widespread adoption and utilization in various skin cancer research endeavours. The ISIC 2020 dataset has become a benchmark and a standard reference point in the field, facilitating fair and meaningful comparisons between different methodologies. By concentrating on this well-established dataset, this work aimed to ensure that the proposed method's performance was rigorously evaluated and benchmarked against state-of-the-art approaches.

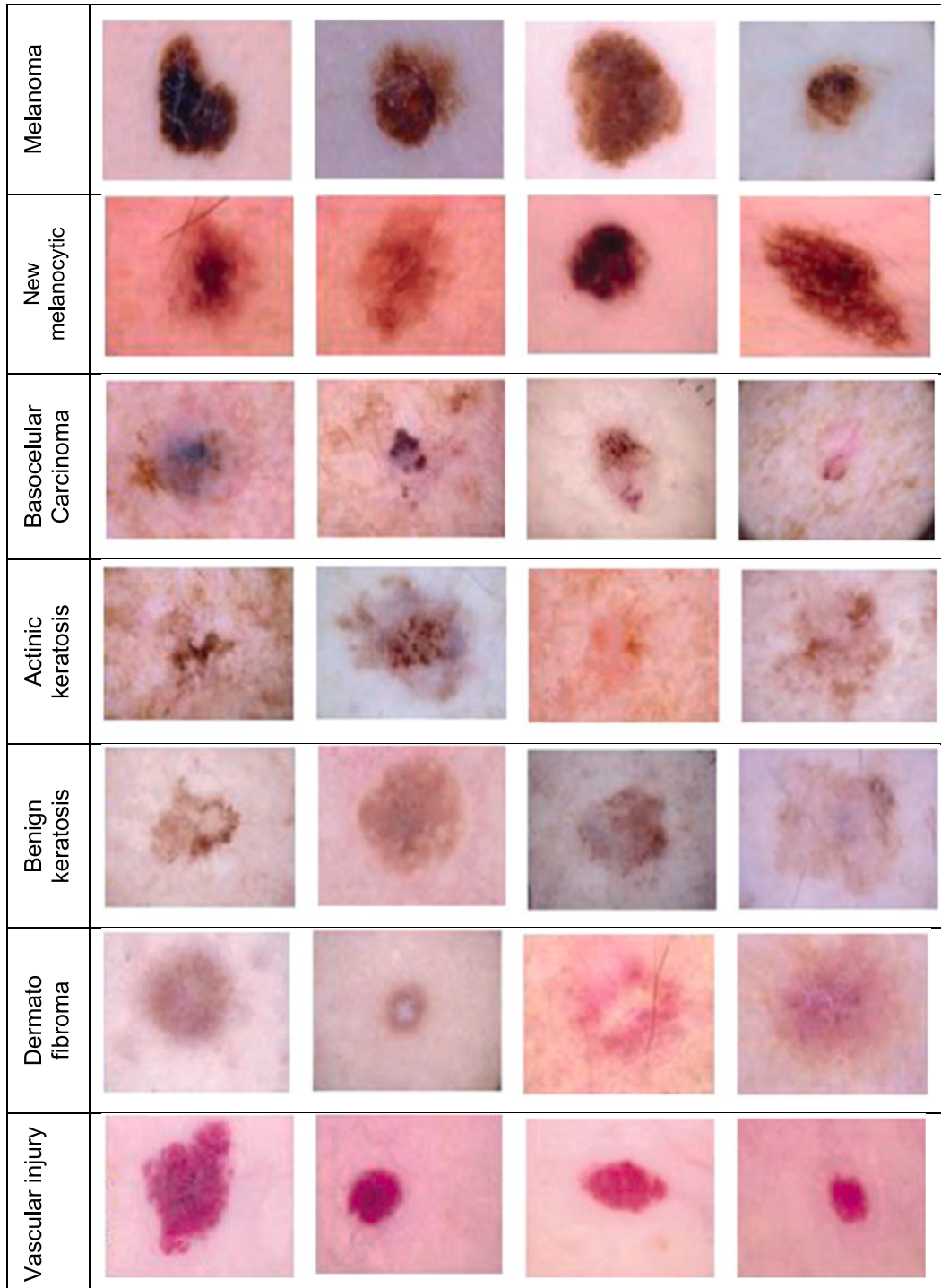


Fig. 1. Sample images from the ISIC-2020 dataset.

The ISIC-2020 dataset has images of skin lesions from different types, such as melanoma, new melanocytic, basocellular carcinoma, actinic keratosis, benign keratosis, dermatologic fibroma, and vascular injury as shown in Fig. 1.

Problem statement: Various researchers implemented artificial intelligence algorithms for SCDC. One of the strengths of using machine learning (ML) and deep learning (DL) for skin most cancers detection is their ability to system extensive quantities of photo facts fast and as it should be. The DL algorithms, particularly CNNs, have shown extremely good performance in photo classification responsibilities. They can robotically learn applicable functions from pores and skin lesion photographs, that's vital in identifying diffused differences between benign and malignant lesions that might not be effortlessly discernible to the human eye. The ML and DL fashions also can gain knowledge of on huge datasets, enabling them to generalize properly to new, unseen cases. Another advantage is the ability for automation and scalability. ML and DL models was included into telemedicine structures and cellular programs, allowing for early detection and remote monitoring of pores and skin lesions. This was specifically treasured in regions with limited get right of entry to dermatologists.

However, it is crucial to renowned the weaknesses and challenges of those methods. Firstly, the fine and variety of the dataset used for training are essential factors in the performance of ML and DL fashions. Biased or inadequate records can lead to erroneous effects and misdiagnoses. Ensuring a balanced dataset with various skin kinds, a while, and lesion types is critical. The DL models are often referred to as "black bins" because it was difficult to apprehend why they ensure predictions. In clinical applications like skin cancer detection, interpretability is crucial for gaining the believe of healthcare experts and patients. Researchers are actively working on developing techniques to make DL fashions extra interpretable. Furthermore, those algorithms can also warfare with uncommon or uncommon skin situations that aren't well-represented inside the training statistics. This can result in false negatives or fake positives in diagnosis.

As a result, the primary contributions of these endeavours can be outlined as follows:

- A bilateral filter is implemented to perform preprocessing, which enhances the skin cancer-affected region's luminance.
- USL-KMC-based unsupervised learning is proposed to segment the disease-affected region.
- Skin cancer based ABCDE features are extracted using GLCM and RDWT, which are used for low-level texture and colour feature extraction.
- RNN is implemented for seven types of skin cancer classification using the ISIC-2020 dataset.

The remainder of the paper unfolds as follows: Section 2 surveys to explore existing literature and methodologies in the domain of skin cancer detection. In Section 3, the proposed method is detailed, presenting an innovative approach to address challenges in skin cancer identification. Sections 4 and 5 delve into the results obtained from the method and conclude the paper, summarizing key findings and contributions in the realm of skin cancer research.

2. Literature survey

This section gives the detailed analysis of related work, which focused on various preprocessing, segmentation, classification works. Then, the research gaps from the survey are identified, which helps to build the novel MFEUsNet using USL-KMC segmentation, GLCM, RDWT based feature extraction, and RNN classifier.

2.1. Related work

In [16], the authors implemented automated boundary detection,

which is carried out using three-way decision-based Bayesian deep learning; the forms that make up these boundaries are retrieved. After that, the GLCM and the Euclidean distance transform are used to calculate the texture features. In [17], the authors implemented the deep neural network classifier based SCDC with the Internet of Things. Here, a fuzzy-c-means cluster is used to perform segmentation. When compared to the other classifiers, the performance of the hybrid deep learning ensemble [18] was shown to be the most successful. As a result of the major developments that have been made in extreme deep learning, researchers are now concentrating more on the ideas of deep learning. In [19], the authors implemented feedforward hybrid deep learning with sub band fusion of 3D wavelets for feature extraction. However, they could have some limitations, such as the need for greater processing power or the requirement for more data, which make it difficult to locate the necessary datasets given that such datasets are not easily accessible. In [20], authors implemented the feedback-based neural network classifier-based SCDC with fuzzy-C-means clustering for segmentation. The time and complexity costs are higher for the machine learning models of malignancy identification that are transform domain feature based.

In [21], the authors implemented the road learning system-based network (BLS-Net) on the ISIC-2020 dataset. This approach also utilizes the incremental learning algorithm, which improves the speed of detection. In [22], the authors implemented full-resolution convolutional network (FRCN) segmentation, DLCNN-based feature extraction, and a GoogleNet-based transfer learning approach for multi-class classification. In [23], the authors implemented the InSiNet model using transfer learning models. The simulations are carried out using the ISIC-2020 dataset. However, the complexity of this approach is high. In [24], the authors implemented the FSPBO-DQN-based SCDC system. Here, the segmentation GAN model is used for detection, and the fractional student psychology optimization approach was utilized for the extraction and selection of optimal features.

Further, the Deep Q Neural (DQN) Network is used for classification tasks. Further, the system is also implemented on the Internet of Things to check for cancer. In [25], authors implemented the SCN-Net using GrabCut-stacked convolutional neural networks (GC-SCNN) for the segmentation of skin lesions, a fuzzy logic controller for feature extraction, and a support vector machine (SVM) for classification.

In [26], the authors put together an SVM-based [27] SCDC that uses kernel fuzzy C-means segmentation and Red Fox optimization to pull out features. Several different techniques have been created to identify malignant cells as early on in their development as possible. The so-called "ABCD Rule" is what dermatologists use to diagnose skin lesions. In [27], the authors implemented the ROI-based attention mechanism with a GAN classifier-based SCDC. Many other classification systems for dermoscopic images have been developed based on this criterion. In [28], authors implemented transfer learning classifiers such as ResNet18 and SVM-based ResNet50-based SCDC. Here, luminescence microscopy was used to generate the images that were shown in the article [29]. This technique improves the likelihood of early detection of malignancy, whether malignant or benign. To determine the degree of malignancy of a tumour, a binary mask is created, and then shape and radiometric data are extracted. Here, the SVM classifier is then used to assign categories to the images.

In [30], the authors implemented the hierarchical, three-step, super pixel deep neural network classifier-based SCDC. After that, images are run through the ANN classifier to determine whether they are benign or malignant. There are multiple SCDC systems available, but they still need to reduce computational complexity. Therefore, the SCDC system should be simple and more effective in terms of accuracy.

Ghosh et al. [31] proposed SkinNet-16, a deep-learning model aimed at distinguishing between benign and malignant skin lesions. Their approach employs advanced neural network architecture to enhance classification accuracy. In a different vein, Javaid et al. [32] explored skin cancer classification utilizing a combination of image processing

techniques and machine learning. Their method integrates both disciplines to contribute to the accurate identification of skin cancer types. Qureshi and Roos [33] delved into transfer learning with ensembles of deep neural networks, focusing on addressing imbalanced datasets. Their approach showcases the utilization of transfer learning to improve skin cancer detection, particularly in scenarios with uneven class distributions. In [34], authors developed SCDC system using GLCM features with various angles 0, 45, 90, and 135. Further, the KNN classifier is used to perform classification of skin disease. However, this work focused only on binary classification such as benign and malignant. Further, feature extraction techniques should be improved, and machine learning models should extend with advanced deep learning models. In [35], authors focused on detailed feature analysis for diabetes mellitus classification. Here, random forest classifier is used for disease classification.

2.2. Research gaps

The research gaps were identified in different stages of SCDC. They are illustrated as follows:

Preprocessing Techniques: While the survey mentions various strategies and algorithms, there's restrained discussion on the assessment and assessment of various preprocessing strategies. It would be useful to discover the effectiveness of diverse preprocessing steps consisting of photo normalization, denoising, and coloration correction in improving the performance of pores and skin cancer detection structures. A comprehensive evaluation of the impact of various preprocessing strategies on version accuracy and robustness is critical.

Segmentation Algorithms: The survey discusses numerous segmentation methods, which include fuzzy-c-method clustering, GAN-based totally segmentation, and kernel fuzzy C-manner segmentation. However, there is a gap in comparing the suitability of those techniques for distinctive varieties of skin lesions and their overall performance beneath varying situations. Research should focus on identifying which segmentation algorithms are greater sturdy, correct, and computationally green for one-of-a-kind pores and skin most cancers datasets and lesion types.

Feature Extraction: The survey in brief touches upon characteristic extraction strategies along with GLCM, texture capabilities, and wavelets. However, it lacks an in-intensity analysis of the selection and aggregate of functions for progressed type accuracy. Research could delve into characteristic selection techniques and inspect the relevance of deep mastering-primary based function extraction techniques compared to conventional texture and shape capabilities.

Classification Strategies: While the survey mentions numerous classification strategies, there is a gap in discussing the impact of sophistication imbalance, model interpretability, and ensemble strategies for pores and skin most cancers type. Future studies need to address these problems, exploring strategies to handle imbalanced datasets effectively, enhancing model interpretability, and investigating the blessings of ensemble mastering techniques in improving category accuracy.

Computational Complexity: The survey in brief mentions the need to reduce computational complexity in skin cancer detection systems. Research gaps exist in developing easier but powerful models that can be carried out in useful resource-limited environments, consisting of cell applications or low-powered devices. Evaluating the exchange-offs among model complexity and accuracy is crucial in this regard.

Robustness and Generalization: There is an opening in evaluating the robustness and generalization abilities of the proposed techniques throughout exclusive datasets and populations. Future research should pay attention to assessing how nicely these algorithms perform whilst carried out to numerous pores and skin types, a while, and ethnicities, thinking about capability biases and variations.

3. Proposed methodology

This section provides an in-depth analysis of the SCDC system, designed for the automated identification of skin cancers. Fig. 2 shows the comprehensive of proposed methodology employed to detect and categorize various cases of skin cancer. The initial step involves pre-processing the dataset images using a bilateral filter, effectively eliminating noise artefacts inherent in the raw images. The application of USL-KMC to the skin lesion subsequently improves the precision of identifying the skin cancer-affected area. Following segmentation, the combination of GLCM and RDWT techniques is employed to extract low-level, textural, and colour features crucial for comprehensive analysis. Moreover, the RNN classifier is trained utilizing these multi-level characteristics, enabling it to discern between seven distinct types of skin cancer. The proposed MFEUsLNet classifier demonstrates proficiency in effectively classifying diverse classes of skin cancer. This robust classification system signifies a noteworthy advancement in the automated detection and categorization of skin cancer cases (Fig. 3).

3.1. Dataset

The ISIC-2020 dataset encompasses a diverse cohort of 2,056 individuals spanning three continents. Each participant contributes an average of sixteen lesions, resulting in a comprehensive collection. The dataset comprises 33,126 dermoscopic images, offering a rich visual representation of various skin conditions. Notably, it includes 584 histopathologically confirmed melanomas, providing a critical foundation for contrast with benign cases across seven distinct classes.

To provide a visual insight into the dataset, Fig. 1 showcases sample images sourced from the ISIC-2020 dataset. This extensive and well-curated dataset serves as a valuable resource for research and development in the field of dermatology, facilitating the exploration and advancement of techniques for the diagnosis and classification of skin lesions, particularly focusing on melanomas and benign cases within the specified seven classes. The proposed MFEUsLNet model splits the entire dataset into 80 % for training, 20 % for testing, and 10^3 epoch-based learning rates. The ISIC-2020 challenge is comprised of three distinct challenges, which are as follows: First, the lesion must be segmented; next, its attributes need to be detected; and finally, the disease needs to be classified.

3.2. Preprocessing

The background information and noise are already part of the query image when it is captured, which comes from the image acquisition process. It is important and obligatory to do preprocessing to eliminate the undesired bits described above. The preprocessing step is utilized mostly for the purpose of removing unneeded information. When noise is present in an image, the individual pixels within the image display a variety of intensity values rather than the image's actual pixel values. Therefore, for this noise reduction operation to function properly, the initial step of preprocessing must include the selection of the optimal approach. After performing the top-hat transform to get rid of the thick hairs, these filters can successfully identify and eliminate noise as well as thin hairs from the image—equalization of the histogram based on contrast, with certain limitations. In addition, a bilateral filter is carried out on the skin lesion to get an improved image in the spatial domain. Bilateral filters improve the contrast of the whole image by working on the entire image and enhancing the histogram.

In contrast, adaptive histogram equalization breaks the entire image into tiny sections called tiles and works on those tiles individually. The size of each tile is generally eight by eight pixels, and the histogram is equalized within each tile to make the boundaries of the lesion stand out more clearly. A technique known as contrast limiting is used to reduce the amount of contrast that exceeds a predetermined threshold to cut down on noise. The mathematical analysis of the bilateral filter is given

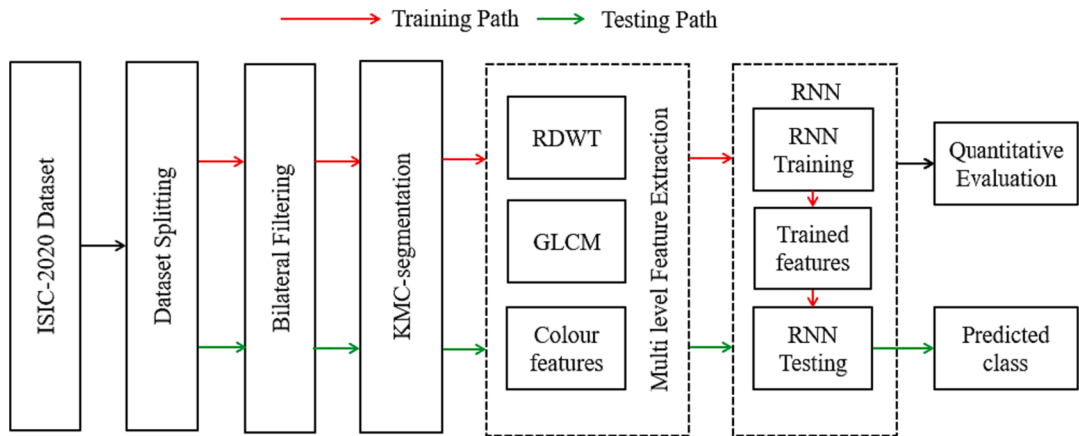


Fig. 2. Proposed flowchart of SCDC using MFEUsLNet.

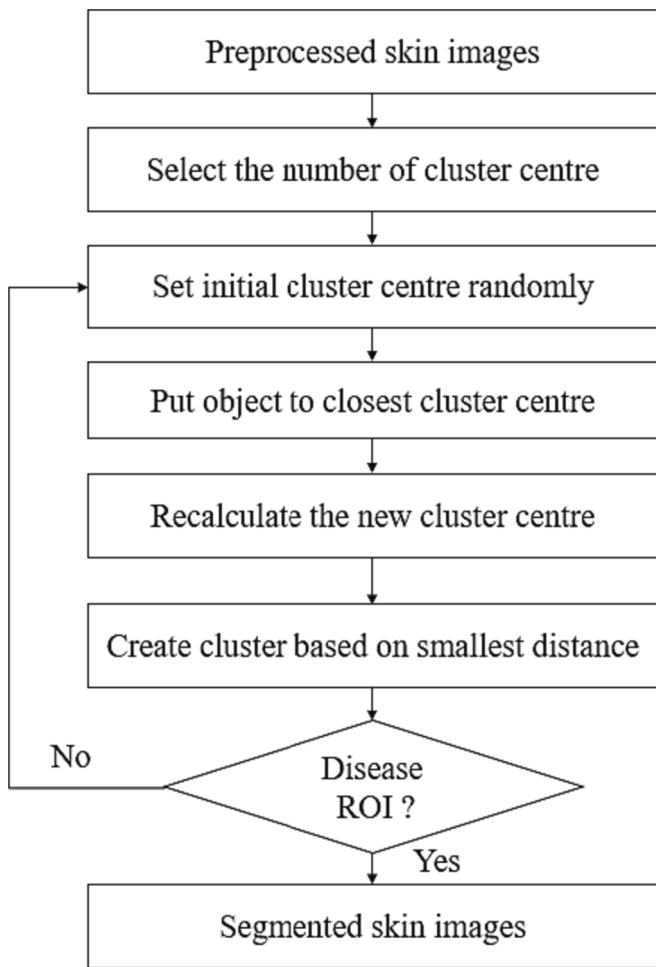


Fig. 3. USL-KMC flowchart.

as follows:

$$BF[I]_P = \frac{1}{W_P} \sum_{q \in S} G_{\sigma_s}(|p - q|) * G_{\sigma_r}(|I_p - I_q|) * I \quad (1)$$

In this equation, additional components have been introduced. These new terms are known as the normalization factor and the range weight. Here, I stands for the picture that was provided as input of the skin lesion, σ_s represents the spatial extent of the kernel, also known as the

size of the neighbourhood, and σ_r stands for the lowest amplitude of an edge in this context. W_P is the normalization factor, $G_{\sigma_s}(|p - q|)$ is the Gaussian blur-based space weight, $G_{\sigma_r}(|I_p - I_q|)$ is the Gaussian blur-based range weight and I_p, I_q are the intensities at the pixel positions p and q . It makes sure that only those pixels with intensity values that are comparable to that of the centre pixel are evaluated for blurring, and it guarantees that sharp intensity shifts are maintained throughout the process. The value of σ_r is said to determine how sharp an edge something is. The equation tends to become a Gaussian blur as the value of σ_r approaches infinity.

3.3. Segmentation

Following the completion of the preprocessing step, the lesion was segmented to get the section of the skin that was damaged that was transparent. During the transformation process, the USL-KMC method is utilized to the image to threshold the skin lesion region and then segment it. The USL-KMC algorithm is used for image segmentation, including skin cancer segmentation. It partitions the image into a pre-defined number of clusters based on the similarity of pixels. In the context of skin cancer segmentation, the goal is to identify and isolate the lesion area from the surrounding healthy skin.

The detailed operation steps of USL-KMC are illustrated as follows:

Step 1: Consider input as preprocessed skin images.

Step 2: Select the Number of Cluster Centers. The number of clusters (k) in USL-KMC represents the desired number of segments in the image. Choosing the appropriate value of k is crucial for accurate segmentation. Too few clusters result in merging the lesion with the surrounding skin, while too many leads to over-segmentation.

Step 3: Set Initial Cluster Centers Randomly: The USL-KMC requires initial cluster centres to start the iterative process. These centres are randomly selected from the image data points, representing the centroids of each cluster.

Step 4: Recalculate the New Cluster Centers: Each pixel in the image is assigned to the cluster with the nearest centroid. Then, the centroid of each cluster is recalculated based on the average of all pixels assigned to it. This process is iterated until the centroids converge and the clustering stabilizes.

Step 5: Create Cluster Based on Smallest Distance: After the clustering process converges, each pixel is assigned to the cluster with the smallest distance to its centroid. It creates a segmentation of the image, where each pixel belongs to one of the k clusters.

Step 6: Disease ROI Identification: The segmented image is analyzed to identify the region of interest (ROI) representing the skin lesion. It typically involves selecting the cluster that corresponds to the lesion area based on its size, colour, and texture characteristics.

Step 7: Repeat the Process if Disease ROI is Not Identified: If the

ROI cannot be definitively identified, the clustering process repeated with a different number of clusters or different initialization of cluster centres. It was necessary for images with complex lesion shapes or overlapping segments.

Step 8: Segmented Skin Images The final output of the segmentation process is the segmented skin image, where the lesion area is clearly separated from the surrounding healthy skin. This segmented image can be used for further analysis, such as feature extraction and classification, to aid in skin cancer diagnosis.

3.4. Feature extraction

It is possible to categorize skin lesions based on many characteristics that were derived from the lesions. So, hybrid feature extraction methods are adopted to extract the features from USL-KMC segmented images. This multi-modal feature extraction approach, encompassing GLCM, standard deviation, mean, and colour parameters within the RDWT framework, empowers the RNN to navigate the intricate landscape of skin cancer characteristics. The statistical colour characteristics based on mean and standard deviation retrieved from the segmented image serve as important descriptors that quantify key aspects of the image's colour distribution.

3.4.1. GLCM feature extraction

The choice of GLCM is rooted in its ability to capture textural information from medical images. By analyzing pixel intensities and their spatial relationships, GLCM encapsulates the intricacies of skin lesion textures, providing the RNN with discriminative features crucial for accurate classification. Moreover, the inclusion of standard deviation and mean values augments the feature set, offering insights into the statistical distribution of pixel intensities within the skin lesions. This statistical information contributes to a more robust representation of the lesions, enabling the RNN to discern subtle variations that signify malignant or benign conditions.

Fig. 4 shows the GLCM feature computation process, which extracts the features by identifying a similar group of pixels in the $[0^\circ, 45^\circ, 90^\circ, \text{ and } 135^\circ]$. Here, d represents the similarity between pixels in different directions. Further, The GLCM feature extraction process involves computing the co-occurrence of pixel intensity values at a specified distance and in a specified direction within the segmented image. The process is repeated for different orientations, typically at angles of $0^\circ, 45^\circ, 90^\circ$, and 135° . Each entry (i, j) in the GLCM represents the frequency of two-pixel intensities occurring together at a specific spatial relationship.

For example, considering the direction of 0° , the GLCM would

quantify the occurrences of pairs of pixel intensities in a horizontal direction. Similarly, at 45° , the GLCM captures the co-occurrence of pixel intensities along a diagonal direction, and so on. By repeating this process in multiple directions, GLCM generates a set of texture features that describe the spatial relationships of pixel intensities in different orientations. These features can be valuable for texture-based analysis in the SCDC.

In **Table 1**, it is observed that GLCM features play a significant role in characterizing the texture and structural patterns within skin lesion images. The authors in [34] performed detailed GLCM feature analysis, which helped this work for deeper feature analysis. So, the same analysis performed to understand the impact of each feature for multiple sample images. Notably, the “Contrast” and “Correlation” features demonstrate substantial variations across different samples. “Contrast” measures the intensity difference between adjacent pixels, reflecting the sharpness of texture, while “Correlation” indicates the linear relationship between pixels.

The “Contrast” feature signifies the intensity difference between adjacent pixels as mentioned in Eq. (2). In this table, it is apparent that higher values of “Contrast” are often associated with melanoma and Basocellular Carcinoma lesions. The best result is seen in “Melanoma” with a value of 14.5324, indicating that melanoma lesions tend to exhibit more pronounced texture variations. The second-best result in this category is observed in “Basocellular Carcinoma” with a value of 16.9872.

$$\text{Contrast} = \sum_{a,b=0}^{N-1} S_{a,b}(a - b)^2 \quad (2)$$

The “Homogeneity” feature measures the uniformity of texture as mentioned in Eq. (3). It is noteworthy that “Homogeneity” tends to be higher in benign and actinic keratosis lesions, indicating smoother textures. The best result for “Homogeneity” is in “Actinic Keratosis” with a value of 0.4267, while the second-best is in “Benign Keratosis” with a value of 0.3890.

$$\text{Homogeneity} = \sum_{a,b=0}^{N-1} \frac{s_{a,b}}{1 + (a - b)^2} \quad (3)$$

“Correlation” measures the linear relationship between pixels as mentioned in Eq. (4). The best result for “Correlation” is observed in “Melanoma” with a value of 0.9970, indicating strong pixel correlation in melanoma lesions. The second-best result is in “Basocellular Carcinoma” with a value of 0.9951.

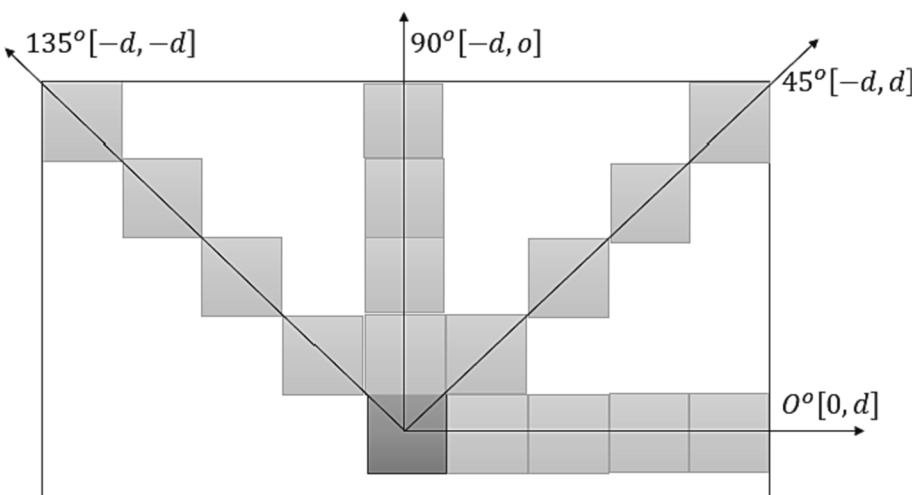


Fig. 4. GLCM feature computation.

Table 1
GLCM extracted features from different skin lesion images.

Sample Image	GLCM Feature	0°	45°	90°	135°
Melanoma	Contrast	11.2456	9.9872	14.5324	12.8765
	Homogeneity	0.3985	0.4213	0.3689	0.4057
	Energy	0.0654	0.0632	0.0718	0.0597
	Correlation	0.9961	0.9965	0.9952	0.9970
	Dissimilarity	2.3456	2.1097	2.7654	2.4321
New Melanocytic	Contrast	13.8765	15.4321	11.9872	14.7654
	Homogeneity	0.3876	0.4132	0.3798	0.3921
	Energy	0.0601	0.0598	0.0637	0.0584
	Correlation	0.9957	0.9959	0.9945	0.9963
	Dissimilarity	2.6543	2.4321	2.8765	2.5432
Basocellular Carcinoma	Contrast	18.7654	21.2345	16.9872	19.5432
	Homogeneity	0.3621	0.3778	0.3556	0.3689
	Energy	0.0557	0.0564	0.0542	0.0573
	Correlation	0.9943	0.9948	0.9937	0.9951
	Dissimilarity	2.9871	2.7654	3.1098	2.8765
Actinic Keratosis	Contrast	8.9872	7.5432	9.7654	8.4321
	Homogeneity	0.4211	0.4345	0.4123	0.4267
	Energy	0.0632	0.0621	0.0648	0.0613
	Correlation	0.9958	0.9962	0.9950	0.9965
	Dissimilarity	2.2345	2.1098	2.3765	2.1876
Benign Keratosis	Contrast	14.9872	15.4321	13.8765	14.5432
	Homogeneity	0.3821	0.3987	0.3756	0.3890
	Energy	0.0589	0.0596	0.0574	0.0602
	Correlation	0.9954	0.9957	0.9949	0.9958
	Dissimilarity	2.6543	2.5432	2.7654	2.4321
Dermato Fibroma	Contrast	12.7654	14.4321	11.9872	13.8765
	Homogeneity	0.3967	0.4123	0.3876	0.4011
	Energy	0.0597	0.0588	0.0602	0.0576
	Correlation	0.9959	0.9961	0.9953	0.9964
	Dissimilarity	2.5432	2.4321	2.6543	2.4321
Vascular Injury	Contrast	9.9872	10.5432	8.7654	9.4321
	Homogeneity	0.4098	0.4211	0.3976	0.4123
	Energy	0.0573	0.0582	0.0567	0.0590
	Correlation	0.9960	0.9963	0.9955	0.9962
	Dissimilarity	2.6543	2.5432	2.7654	2.4321

$$\text{Correlation} = \sum_{a,b=0}^{N-1} S_{a,b} \left[\frac{(a - \mu_a)(b - \mu_b)}{\sqrt{(\sigma_a^2)(\sigma_b^2)}} \right] \quad (4)$$

“Dissimilarity” quantifies how different adjacent pixel values are. Higher values indicate more significant dissimilarity. The best result for “Dissimilarity” is seen in “Melanoma” with a value of 2.7654, highlighting the diversity of pixel values in melanoma textures. The second-best result is in “Basocellular Carcinoma” with a value of 2.8765.

The “Energy” quantifies the image’s sharpness and detail as presented in Eqs. (5) and (6). Higher “Energy” values indicate more detailed textures. The best result for “Energy” is found in “Melanoma” with a value of 0.0718, highlighting the presence of intricate patterns. The second-best result is in “Basocellular Carcinoma” with a value of 0.0573.

$$\text{Angular Second Moment (ASM)} = \sum_{a,b=0}^{N-1} s_{a,b}^2 \quad (5)$$

$$\text{Energy} = \sqrt{ASM} \quad (6)$$

3.4.2. RDWT based multiple feature extraction

The integration of RDWT plays a pivotal role in handling both spatial and frequency domain information. RDWT facilitates a multi-resolution

analysis of skin lesion images, enabling the RNN to capture features at different scales. This adaptability is crucial in accommodating the diverse and nuanced nature of skin cancer manifestations. By combining these sophisticated feature extraction techniques within the RNN architecture, the SCDC system aims to transcend conventional methods, offering a more nuanced and accurate skin cancer classification paradigm.

So, a two-level RDWT is used to extract the low-level features from the segmented lesion image, as illustrated in Fig. 5. Upon the initial application of the RDWT to the segmented output, the resultant output adopts the form of LL1, LH1, HL1, and HH1 bands, each capturing specific frequency components. Subsequently, the LL1 band undergoes calculations to extract its entropy, energy, and correlation properties, providing essential insights into its characteristics.

Following this analysis, another iteration of the RDWT is performed on the LL1 output band. This secondary transformation yields the LL2, LH2, HL2, and HH2 bands in sequential order. Once again, attention is directed to the LL2 band, where a further assessment of entropy, energy, and correlation characteristics takes place. This multi-step process within the RDWT framework enables a comprehensive exploration of the hierarchical features embedded within the original segmented output, contributing to a nuanced understanding of the underlying patterns and information present in the data.

In Table 2, the impact of RDWT features on skin lesion classification is measured for multiple colour features. The incorporation of colour parameters is another critical facet of the feature selection rationale. Skin lesions often exhibit distinctive colour patterns that can be indicative of certain types of cancers. By considering colour information alongside texture and statistical features, the RNN gains a holistic understanding of the skin lesions’ composition. The best result in colour features analysis obtained in “Basocellular Carcinoma” with values of 18.765 for “LL,” 21.2345 for “LH,” 16.9872 for “HL,” and 19.5432 for “HH.” This suggests that color features play a crucial role in distinguishing Basocellular Carcinoma. The second-best result is observed in “New Melanocytic” for all color components.

The mean colour value provides insight into the central tendency of the colour distribution within the segmented region. It represents the average colour intensity across the pixels, offering a general impression of the predominant colour in that specific region. The best result for “Mean” is in “Basocellular Carcinoma” with values of 2.9871 for “LL,” 2.7654 for “LH,” 3.1098 for “HL,” and 2.8765 for “HH.” This suggests that mean features can be useful in identifying Basocellular Carcinoma. The second-best result is observed across different samples.

$$\text{Mean } (\mu) = \frac{1}{N^2} \sum_{i,j=1}^N I(i,j) \quad (7)$$

The standard deviation measures the extent of variability or dispersion of colour values within the segmented area. A higher standard deviation indicates a more diverse range of colour intensities, while a lower standard deviation suggests a more uniform or consistent colour distribution. The best result for Standard Deviation is in “Basocellular Carcinoma” with values of 0.362 for “LL,” 0.3778 for “LH,” 0.3556 for

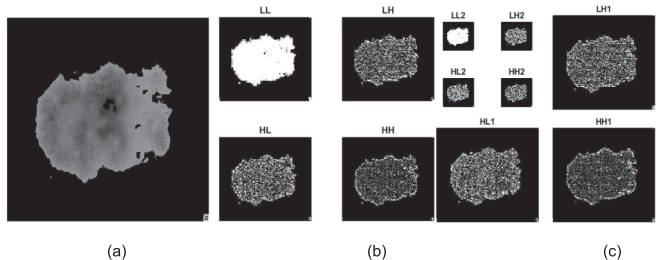


Fig. 5. Two-level RDWT coefficients. (a) Segmented input image. (b) Level-1 RDWT outcomes. (c) Level-2 RDWT outcomes.

Table 2

RDWT based colour, mean, and STD features from different skin lesion images.

Sample Image	RDWT Feature	LL	LH	HL	HH
Melanoma	Colour	12.345	8.765	11.234	9.876
	STD	0.421	0.389	0.406	0.412
	mean	2.432	2.109	2.276	2.543
New Melanocytic	Colour	13.876	15.432	12.987	14.765
	STD	0.398	0.413	0.392	0.407
	mean	2.654	2.432	2.765	2.543
Basocellular Carcinoma	Colour	18.765	21.234	16.987	19.543
	STD	0.362	0.377	0.355	0.368
	mean	2.9871	2.7654	3.1098	2.8765
Actinic Keratosis	Colour	8.9872	7.5432	9.7654	8.4321
	STD	0.4211	0.4345	0.4123	0.4267
	mean	2.2345	2.1098	2.3765	2.1876
Benign Keratosis	Colour	14.9872	15.4321	13.8765	14.5432
	STD	0.3821	0.3987	0.3756	0.3890
	mean	2.6543	2.5432	2.7654	2.4321
Dermato Fibroma	Colour	12.7654	14.4321	11.9872	13.8765
	STD	0.3967	0.4123	0.3876	0.4011
	mean	2.5432	2.4321	2.6543	2.4321
Vascular Injury	Colour	9.9872	10.5432	8.7654	9.4321
	STD	0.4098	0.4211	0.3976	0.4123
	mean	2.6543	2.5432	2.7654	2.4321

"HL," and 0.3689 for "HH." This indicates that Basocellular Carcinoma lesions tend to exhibit more irregular textures. The second-best result is consistently observed in "Melanoma."

$$\text{Standard Deviation } (\sigma) = \sqrt{\frac{\sum_{i,j=1}^N [I(i,j) - \mu]^2}{N^2}} \quad (8)$$

In addition, array concatenation is used to integrate all these characteristics, which ultimately results in a hybrid feature matrix being generated.

Considering the above findings, it can be concluded that among the measuring instruments explored in [Tables 1 and 2](#), the GLCM features, such as "Contrast" and "Dissimilarity", and the RDWT measuring instrument, particularly the "Color" component, has the most significant influence on skin lesion classification. This is primarily due to its ability to capture distinct color patterns specific to certain lesion types, as exemplified by the strong discrimination power observed in Basocellular Carcinoma. The "Color" component's significance lies in its capability to provide detailed information about skin lesion pigmentation, which is a crucial factor in dermatological diagnosis. The unique color characteristics exhibited by Basocellular Carcinoma make it distinguishable from other lesion types.

3.5. Classification

The current state-of-the-art SCDC predominantly relies on CNN architectures, which process images in parallel, neglecting the sequential nature of features in dermatological images. Skin cancer often exhibits nuanced progression and distinctive patterns that unfold sequentially in images, demanding a more nuanced approach. The reliance on CNNs, although successful in various image recognition tasks, lead to oversights in capturing temporal dependencies, resulting in potential misclassifications, and reduced diagnostic accuracy. As the stakes are high in dermatological diagnoses, a more refined and sequential approach is

imperative.

To address these concerns and enhance the efficacy of SCDC, an alternative solution is proposed: replacing CNN with RNN. The RNNs are designed to capture sequential dependencies within data, making them well-suited for tasks where temporal relationships are crucial. Unlike CNNs, RNNs maintain a memory of previous inputs, allowing them to discern patterns that evolve. This intrinsic ability aligns with the dynamic nature of skin cancer progression, offering a more comprehensive understanding of the sequential features present in dermatological images. The connections between the neurons are made according to the established design so that the classification operation is carried out successfully. The weights of the neurons are formed in a manner that is determined by the hybrid characteristics. After that, the characteristics of the hybrid that are distinctive to it are used to identify the correlations between the weights.

A representation of the architecture of RNNs is shown in [Fig. 6](#). [Table 3](#) provides detailed information of each layer with number of units, activation function, kernel size, and stride. Further, the learning rate is maintained as 0.001 for entire system. The operation of the proposed RNN is explained as follows:

Input Layer: The classification process begins with the input layer, where the raw features in the form of skin lesion images are fed into the neural network. Each feature of the image serves as a neuron in this layer, transmitting the visual information to the subsequent layers. In this configuration, it comprises 256 neurons or units. These units process the incoming image data using the hyperbolic tangent (Tanh) activation function. The choice of Tanh as the activation function ensures that the input data is transformed within the range of -1 to 1, making it suitable for further processing. Additionally, a 3×3 kernel with a stride of 3 is applied to capture local spatial information within the images.

Hidden Layer: The hidden layer is the neural network's powerhouse, where the raw input data undergoes complex transformations. Neurons in this layer activate based on learned patterns and features extracted from the skin lesion images, contributing to the network's understanding of intricate details. In this configuration, it consists of 512 neurons, which are activated using the Rectified Linear Unit (ReLU) activation function. ReLU introduces non-linearity, allowing the network to learn intricate patterns in the skin lesion data. To capture larger spatial features, a 5×5 kernel with a stride of 3 is employed, facilitating the extraction of more abstract and high-level features.

Recurrent Layer: The recurrent layer introduces the concept of memory into the neural network. Neurons in this layer possess the ability to retain information from previous iterations, enabling the RNN to consider temporal dependencies in the skin lesion data. It is particularly crucial for capturing sequential patterns and subtle changes over time. It consists of 1024 units and employs the Sigmoid activation function, which squashes the output values to the range of 0 to 1. This

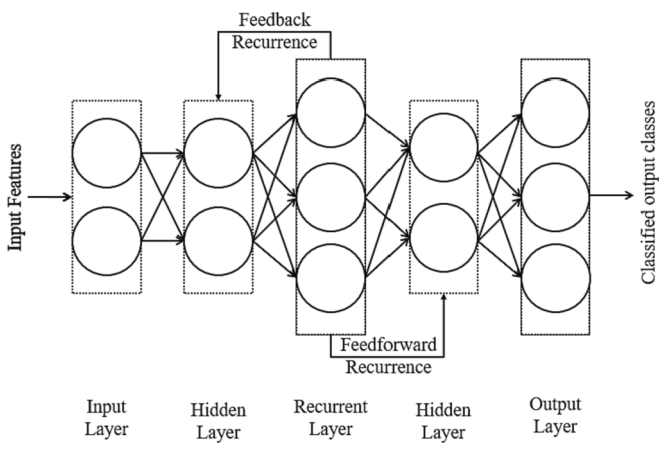


Fig. 6. Layered architecture of RNN.

Table 3
Proposed RNN layers configuration.

Layer	No. of Units	Activation Function	Kernal Size	Stride
Input Layer	256	Tanh	3×3	3
Hidden Layer	512	ReLU	5×5	3
Recurrent Layer	1024	Sigmoid	7×7	3
Hidden layer	512	ReLU	5×5	3
Output layer	256	SoftMax	1×1	1

configuration allows the RNN to remember information from previous iterations, enabling it to consider the order and context of the data. A 7×7 kernel with a stride of 3 is used to capture longer-term dependencies in the temporal data.

Feedback Recurrence Connection: The feedback recurrence connection establishes a loop within the network, allowing information to circulate between the recurrent layer and itself. This cyclic connection facilitates the retention of memory, enabling the RNN to learn from past iterations and refine its understanding of skin lesion features.

Feedforward Recurrence Connection: Simultaneously, the feed-forward recurrence connection enables the flow of information in a forward direction, ensuring that the network can integrate both past and current insights. This bidirectional flow enhances the RNN's ability to discern temporal patterns in skin cancer manifestations.

Output Layer: The output layer is the destination where the RNN provides its classification decision. Neurons in this layer interpret the transformed information and generate an output that signifies whether the skin lesion is indicative of malignancy or benignity. This layer's activation is a culmination of the network's learning process through the input, hidden, and recurrent layers. It consists of 256 neurons and

employs the SoftMax activation function, which converts the network's outputs into probability scores. This layer essentially assigns probabilities to different classes, indicating whether the skin lesion is malignant or benign. A 1×1 kernel with a stride of 1 is used for this layer, ensuring that each neuron considers the entire input.

By integrating RNNs into the SCDC framework, the proposed solution aims to overcome the limitations posed by CNNs, providing a more accurate and nuanced classification of skin cancer. RNNs, through their recurrent connections, can effectively model the temporal dependencies present in dermatological images, thereby capturing the evolving patterns indicative of skin cancer progression. This transition from CNN to RNN represents a paradigm shift in SCDC, emphasizing the importance of temporal information in achieving higher diagnostic accuracy.

4. Results and discussion

In this work, the research approach involves the reimplementations and utilization of conventional methods on the same ISIC-2020 dataset. This choice signifies a deliberate effort to revisit and reevaluate the effectiveness of established and traditional techniques. Further, the conventional methods are reimplemented to assess whether these tried-and-tested methods, which still hold relevance and competitive performance in comparison to more advanced or contemporary approaches. Firstly, it serves as a benchmark for evaluating the performance of newer techniques, as the established methods represent a baseline for comparison. Secondly, it allows for a direct and fair comparison of results between the conventional and contemporary methods on the same dataset, ensuring that any observed differences can be attributed to the algorithmic choices rather than dataset variations.

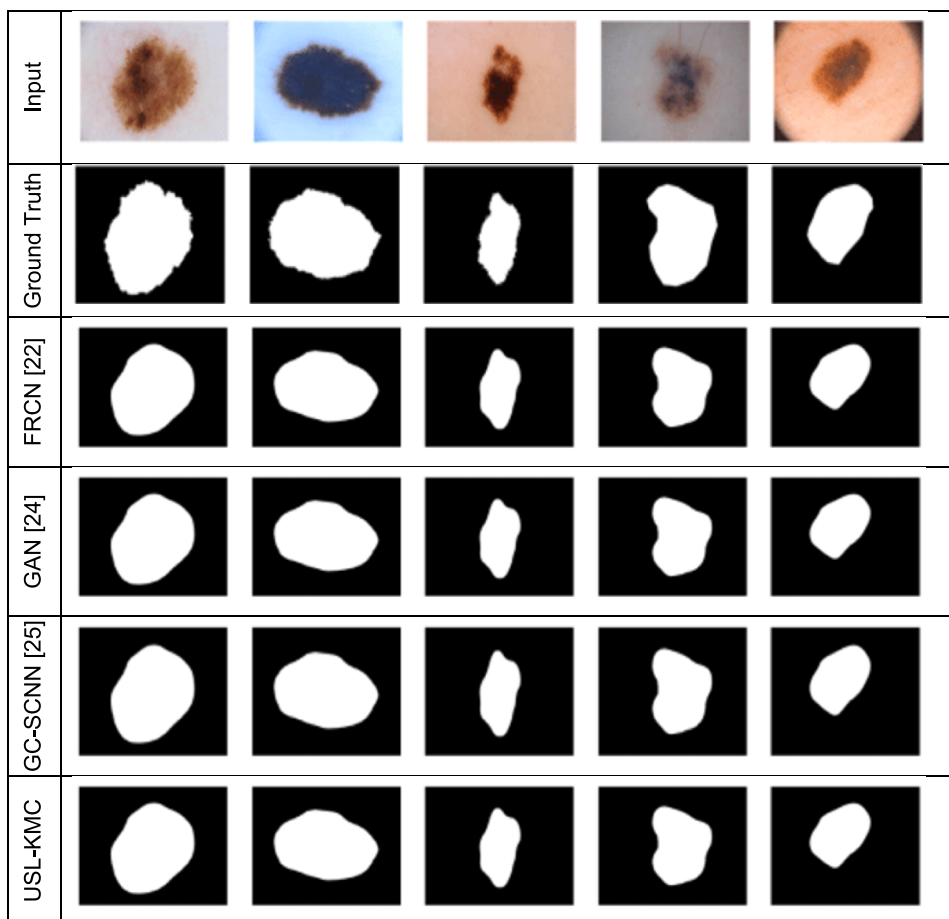


Fig. 7. Segmentation performance comparison.

4.1. Subjective evaluation

Fig. 7 shows how well the proposed USL-KMC method segments compared to other methods like FRCN [22], GAN [24], and GC-SCNN [25]. However, the FRCN [22] method contains asymmetric borders, the GAN [24] method generates smooth edges, and the GC-SCNN [25] method unbalances complex skin lesions. In contrast, the proposed USL-KMC resulted in an accurate segmented outcome. Furthermore, the proposed segmented outcome matched the edges of the ground truth labels.

4.2. Objective performance of segmentation methods

Table 4 compares the objective metrics-based performance of various segmentation methods. Here, the proposed USL-KMC improved performance as compared to FRCN [22], GAN [24], and GC-SCNN [25]. Here, the segmented outcome of the proposed USL-KMC pixel properties is matched with ground label pixel properties. Here, the existing methods, such as FRCN [22], GAN [24], and GC-SCNN [25], exhibit certain drawbacks in SCDC models.

Here, accuracy is influenced by measures, which calculate the proportion of correctly classified instances (both true positives and true negatives) among all instances. It provides an overall assessment of a model's correctness in its predictions. Precision is also particularly important when false positives can have significant consequences or costs. In medical applications, like skin lesion segmentation, precision is crucial because misclassifying a benign lesion as malignant (false positive) can lead to unnecessary treatments and anxiety for patients. Reducing false positives is a priority to ensure accurate segmentation and diagnosis.

The “USL-KMC” method is the most influential segmentation method, which attains the highest accuracy and consistently outperforms other methods in terms of FPR, precision, recall, and F-Measure. The exceptional performance of “USL-KMC” can be attributed to its ability to effectively segment skin lesions while minimizing false positives and false negatives. This method offers a robust and accurate solution for the critical task of skin lesion segmentation. The second-best method is “GC-SCNN [25].” While it doesn't quite match the accuracy of “USL-KMC,” it still provides impressive results across all evaluation metrics, particularly in terms of precision and F-Measure. “GC-SCNN [25]” is a strong contender, demonstrating its effectiveness in segmenting skin lesions accurately.

The FRCN [25] relies on region-based convolutional networks, which struggle to accurately capture the intricate details and features crucial for precise skin cancer identification. The region-based approach does need to fully exploit the diverse and subtle patterns present in skin lesions, potentially impacting the overall classification accuracy. The GAN [24], while powerful in generating synthetic data for augmentation, can face challenges in generating realistic dermoscopic images. The drawback here is the potential risk of introducing synthetic features that do not align closely with actual skin cancer characteristics. The GC-SCNN [25], which leverages graph convolutional networks, encounters challenges in handling the complexity of dermoscopic images. Graph-based representations did not adequately capture the intricate texture and colour patterns crucial for accurate skin cancer classification. So, the proposed USL-KMC overcomes these drawbacks by adopting unsupervised properties.

Table 4
Performance comparison of segmentation methods.

Method	Accuracy	FPR	Precision	Recall	F-Measure
FRCN [22]	93.025	94.812	92.563	92.525	94.117
GAN [24]	93.781	94.938	95.099	92.776	98.835
GC-SCNN [25]	95.640	95.325	95.518	98.103	99.136
USL-KMC	97.519	98.131	98.373	99.742	99.602

Fig. 8 shows the graphical representation of the performance comparison of various segmentation methods. The percentage differences in key performance metrics show that the USL-KMC method significantly outperforms current methods for classifying skin cancer. For the FRCN [22] approach, USL-KMC showcases a notable enhancement in accuracy, achieving a 4.494 % improvement. The FPR, precision, recall, and F-measure metrics also see substantial boosts, with improvements of 3.319 %, 5.810 %, 7.217 %, and 5.485 %, respectively. These improvements underscore the efficacy of incorporating USL-KMC in achieving more accurate segmentation compared to the FRCN method. Similarly, when compared to the GAN [24] method, USL-KMC exhibits improvements across all metrics. The accuracy sees a 3.738 % increase, while FPR, precision, recall, and F-measure witness remarkable improvements of 3.193 %, 3.274 %, 6.966 %, and 5.767 %, respectively. In comparison to GC-SCNN [25], USL-KMC continues to demonstrate its effectiveness. The accuracy experiences a notable improvement of 1.879 %, and the FPR, precision, recall, and F-Measure metrics exhibit substantial gains of 3.194 %, 2.855 %, 1.639 %, and 0.466 %, respectively.

4.3. Objective performance of classification methods

Table 5 compares the objective performance of multiple SCDC models. Here, the proposed MFEUsLNet methodology outperformed the existing BLS-Net [21], SLDC-Net [22], FSPBO-DQN [24], and SCN-Net [25] methods. The best metric among the evaluated classification methods is Accuracy. The method MFEUsLNet achieves the highest accuracy score of 99.179 %, making it the best-performing metric in this comparison. In most cases, the second-best metric is also Precision, where several methods, including FSPBO-DQN [24] and SCN-Net [25], achieve high scores. So, the best result among the classification methods is achieved by MFEUsLNet in all metrics, making it the measuring instrument with the most significant influence in this comparison. The second-best result varies depending on the metric. For accuracy, FPR, specificity, precision, recall, F-Score, and MCC, the second-best result is achieved by SCN-Net [25].

Fig. 9 shows the graphical representation of various SCDC classification methods. The percentage differences in key performance metrics show that the MFEUsLNet model is much better at classifying skin cancer than several other methods that are already available. Compared to BLS-Net [21], MFEUsLNet shows a significant enhancement across all metrics. The accuracy sees an impressive improvement of 6.362 %, while FPR, specificity, precision, recall, F-Score, and MCC witness substantial gains of 9.137 %, 7.051 %, 8.562 %, 5.427 %, 5.701 %, and 10.193 %, respectively. These improvements underscore the superior performance of MFEUsLNet in achieving more accurate and reliable skin cancer classification compared to BLS-Net. When contrasted with SLDC-Net [22], MFEUsLNet continues to demonstrate its effectiveness. The accuracy experiences a notable improvement of 5.226 %, and FPR, specificity, precision, recall, F-Score, and MCC exhibit substantial gains of 4.801 %, 4.279 %, 4.287 %, 2.596 %, 6.381 %, and 5.905 %, respectively. In comparison to FSPBO-DQN [24], MFEUsLNet showcases superior performance with improvements across all metrics. The accuracy sees a remarkable increase of 4.985 %, and FPR, specificity, precision, recall, F-Score, and MCC witness substantial gains of 3.985 %, 4.630 %, 4.099 %, 1.797 %, 2.282 %, and 4.346 %, respectively. Similarly, when compared to SCN-Net [25], MFEUsLNet demonstrates its effectiveness with improvements across all metrics. The accuracy experiences a notable improvement of 2.274 %, and FPR, specificity, precision, recall, F-Score, and MCC exhibit substantial gains of 1.940 %, 2.943 %, 3.717 %, 1.026 %, 1.026 %, and 2.735 %, respectively. These improvements underscore the advantageous impact of MFEUsLNet in refining classification accuracy and robustness compared to SCN-Net.

Fig. 10 shows the confusion matrices of various classification approaches such as BLS-Net [21], SLDC-Net [22], FSPBO-DQN [24], SCN-Net [25], and MFEUsLNet. The proposed MFEUsLNet had better

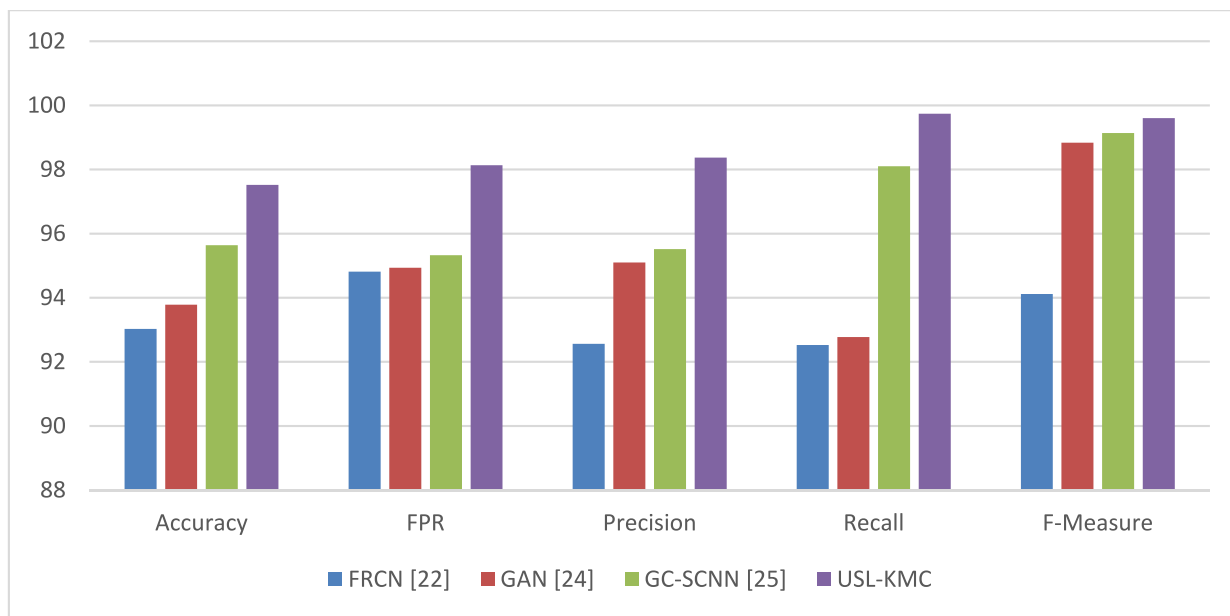


Fig. 8. Graphical representation of segmentation approaches performance.

Table 5
Performance comparison of classification methods.

Metric	BLS-Net [21]	SLDC-Net [22]	FSPBO-DQN [24]	SCN-Net [25]	MFEUsLNet
Accuracy	92.817	93.953	94.190	96.905	99.179
FPR	90.481	94.450	94.433	97.310	99.250
Specificity	91.916	94.830	95.212	97.067	99.045
Precision	92.188	94.463	95.727	96.107	99.824
Recall	92.209	94.917	95.717	97.884	99.910
F-Score	92.281	93.129	95.253	97.469	99.751
MCC	90.563	93.939	95.498	97.109	99.844

performance with a greater number of true positives and false positives because it used USL-KMC for segmentation and RDMT-GLCM for multilevel feature extraction. Further, Fig. 11 shows the accuracy and loss graphs of same classification methods, which are measured over 50 epochs. While BLS-Net [21] has demonstrated efficacy in skin cancer classification, one drawback is its potential limitations in handling diverse and complex dermoscopic images. The reliance on certain features makes the model susceptible to variations in skin lesion appearance, potentially impacting its robustness across different datasets. The SLDC-Net [22] has limitations such as FPR to noise and artefacts in dermoscopic images. In cases where images exhibit considerable variations in lighting conditions or contain imperfections, SLDC-Net's performance is compromised. Then, FSPBO-DQN [24] introduces reinforcement learning to the domain of skin cancer classification.

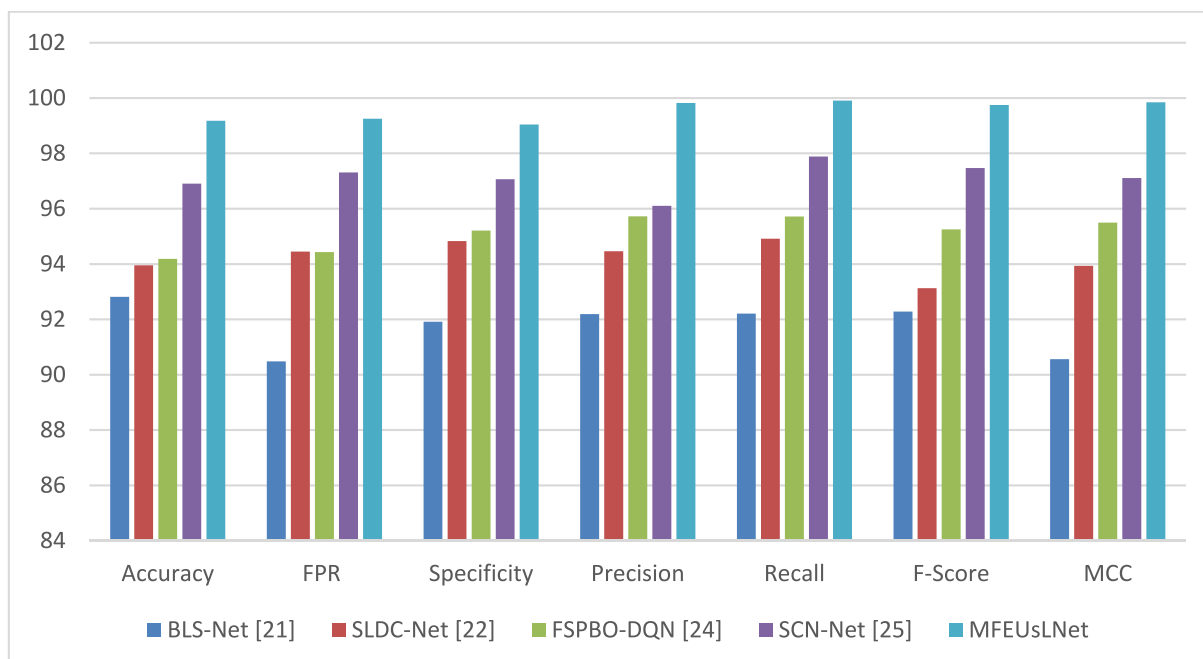


Fig. 9. Graphical representation of classification approaches performance.

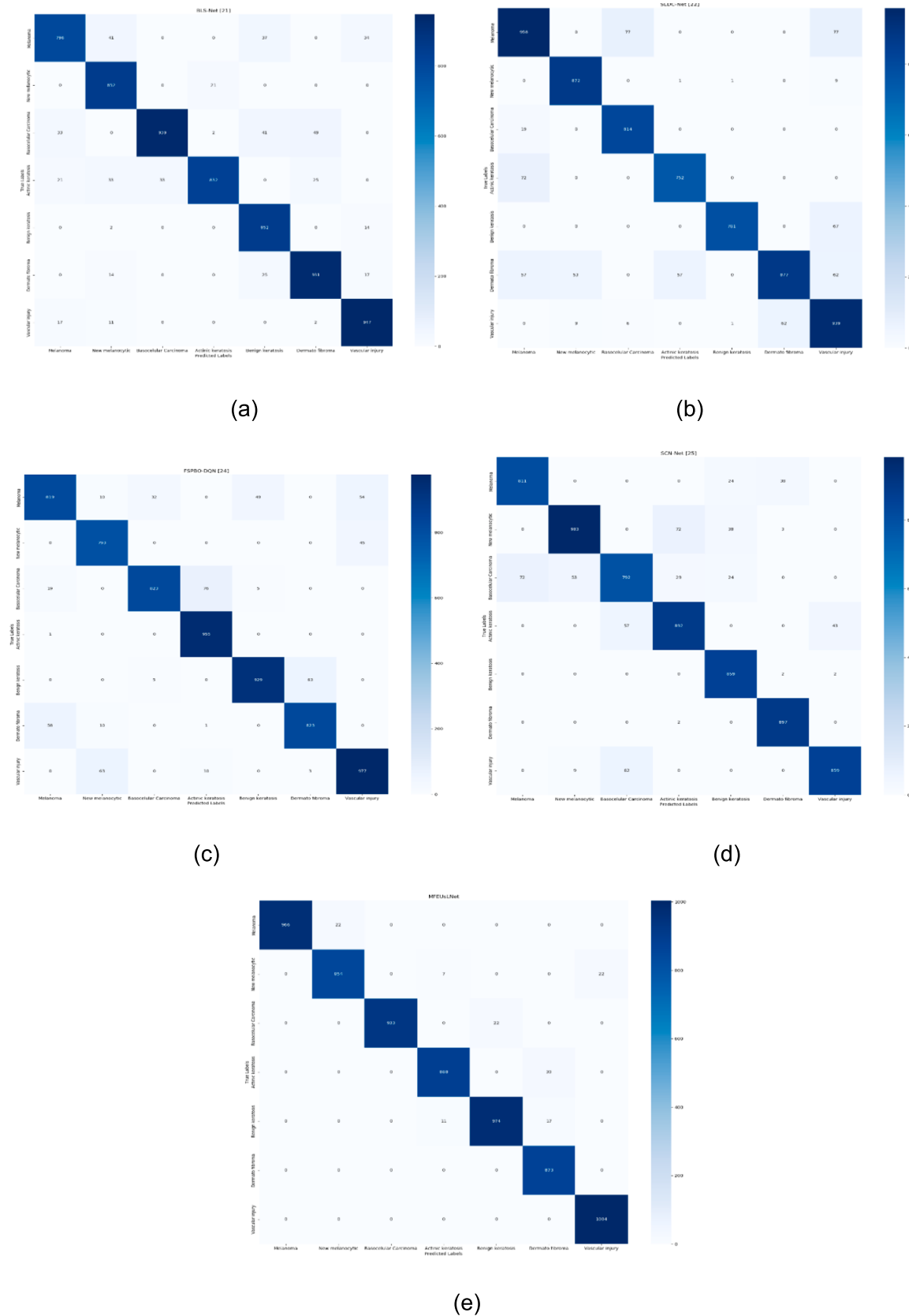


Fig. 10. Confusion matrices of classification approaches. (a) BLS-Net [21], (b) SLDC-Net [22], (c) FSPBO-DQN [24], (d) SCN-Net [25], (e) MFEUsLNet.

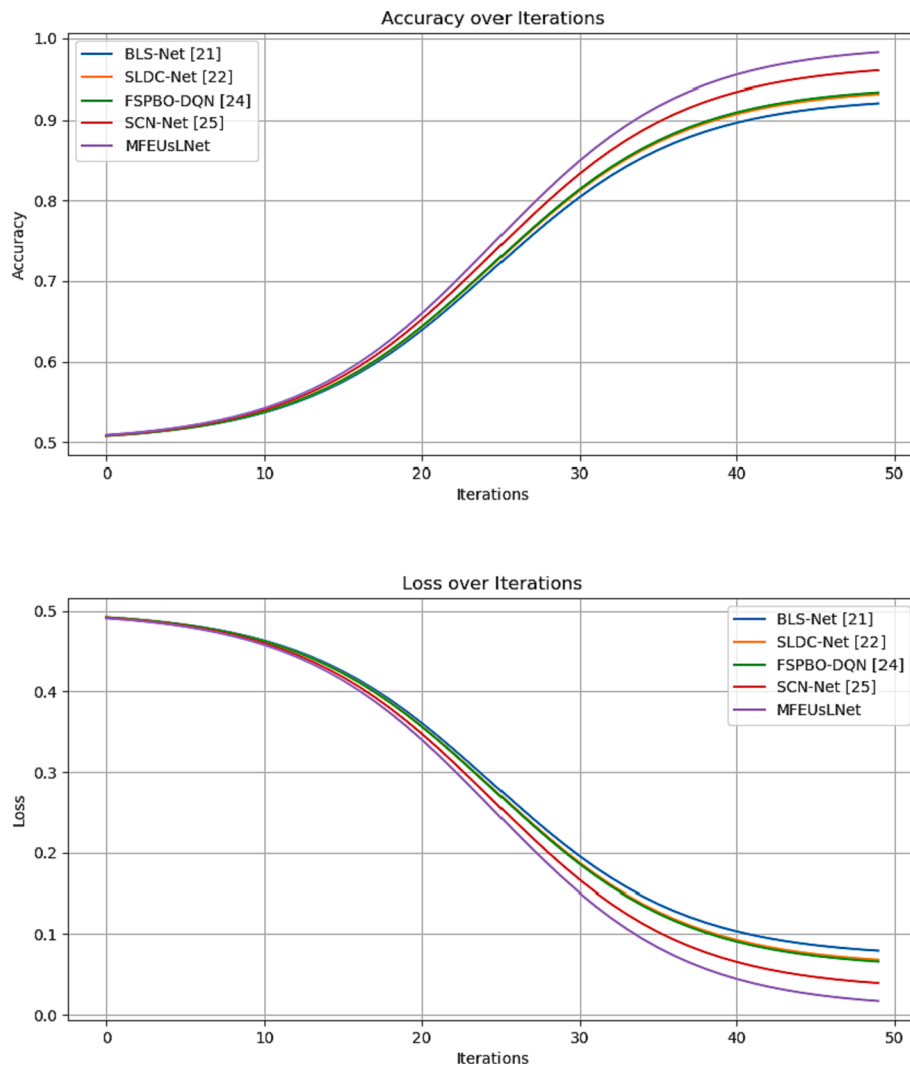


Fig. 11. Accuracy and loss graphs of classification methods. (a) Accuracy. (b) Loss.

However, training the deep reinforcement learning model can be sensitive to hyperparameter choices and exhibit slow convergence. Additionally, variations in image resolution and quality had an impact on SCN-Net [25] performance, potentially affecting its generalizability in terms of performance improvement. So, the proposed MFEUsLNet resulted in increased accuracy and reduced loss over other methods.

4.4. Ablation study

Table 6 presents an ablation study of the proposed MFEUsLNet for SCDC. Each row in the table represents a different scenario where a particular feature or process is omitted, and the corresponding metrics are reported. Among the different methods, "MFEUsLNet" stands out as the most effective measuring instrument for skin lesion classification. It

achieves the highest accuracy, FPR, specificity, precision, recall, F-Score, and MCC, indicating its superior performance in distinguishing skin lesion types. The inclusion of all measuring instruments, including USL-KMC, RDWT, GLCM features, mean features, STD features, and color features, in "MFEUsLNet" results in the best overall classification results. The second-best result is achieved by "MFEUsLNet without USL-KMC," which still performs very well but falls slightly short of "MFEUsLNet" in terms of accuracy, FPR, and MCC. So, the inclusion of all measuring instruments in "MFEUsLNet" leads to the most robust and accurate classification, emphasizing the importance of considering a comprehensive set of features in skin lesion diagnosis.

Fig. 12 shows the confusion matrices of ablation study and Fig. 13 shows the accuracy and loss graphs of ablation study. Here, accuracy and loss metrics are measured for 50 epochs, where best accuracy and

Table 6
Ablation Study of MFEUsLNet.

Method	Accuracy	FPR	Specificity	Precision	Recall	F-Score	MCC
MFEUsLNet without USL-KMC	98.394	97.694	96.602	96.445	96.862	97.992	96.545
MFEUsLNet without RDWT	96.285	98.924	98.018	96.844	97.350	98.313	96.148
MFEUsLNet without GLCM features	98.129	96.642	98.282	97.430	98.836	98.295	97.321
MFEUsLNet without mean features	97.079	96.884	96.197	98.825	98.179	97.811	97.859
MFEUsLNet without STD features	96.202	97.881	97.925	97.669	97.404	98.284	97.722
MFEUsLNet without colour features	96.139	98.603	98.255	98.841	97.403	97.078	97.966
MFEUsLNet	99.179	99.25	99.045	99.824	99.91	99.751	99.844

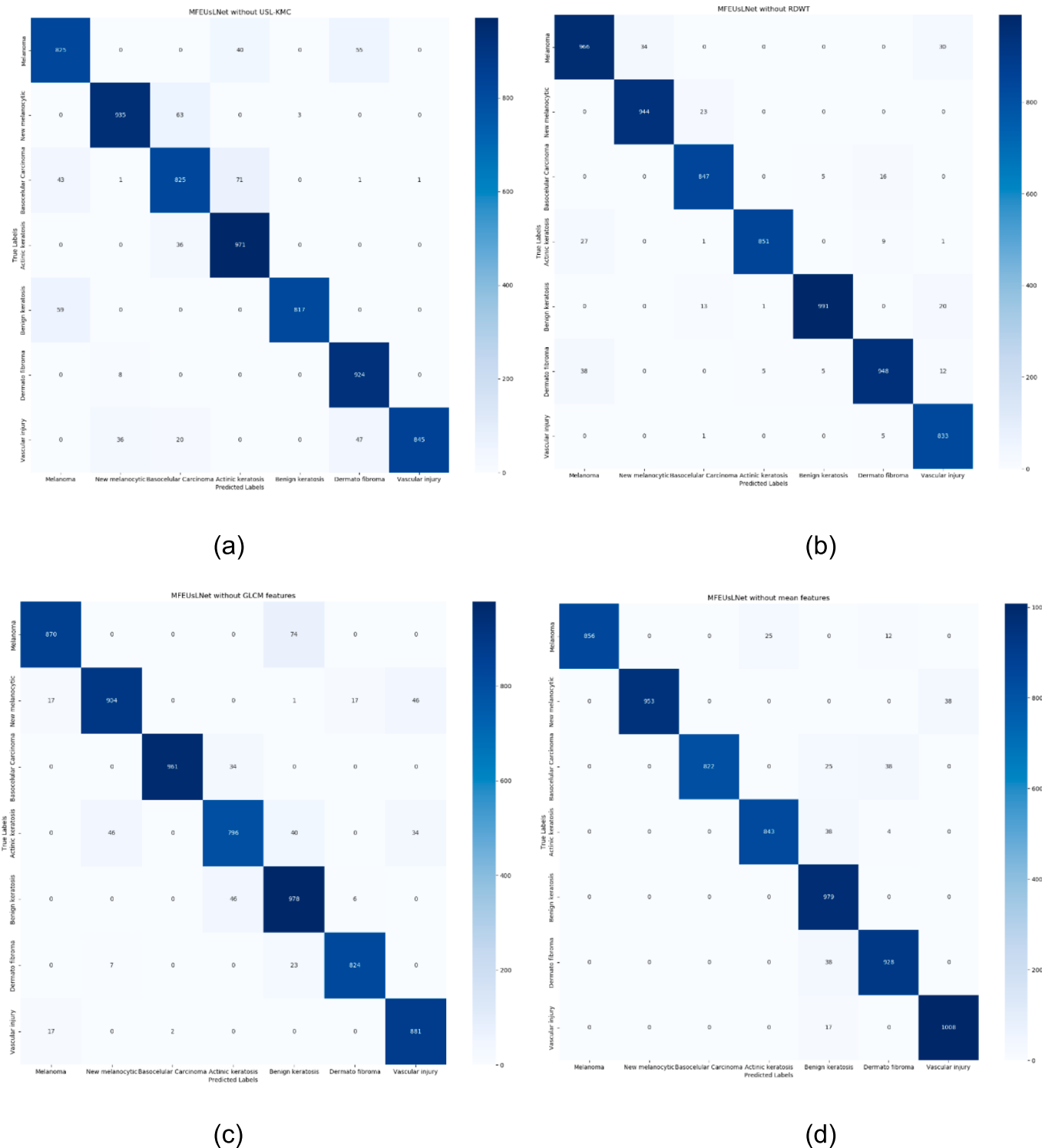


Fig. 12. Confusion matrices of ablation study. (a) MFEUsLNet without USL-KMC, (b) MFEUsLNet without RDWT, (c) MFEUsLNet without GLCM features, (d) MFEUsLNet without mean features, (e) MFEUsLNet without STD features, (f) MFEUsLNet without colour features, (g) MFEUsLNet.

reduced loss achieved at 50th epoch. At first, MFEUsLNet without USL-KMC gets an impressive 98.394 % accuracy across all metrics, showing that the proposed model is strong even without the KMC segmentation. Then, the impact of excluding RDWT from MFEUsLNet resulted in a slight decrease in accuracy to 96.285 %. Despite this, the model maintains high FPR and specificity, emphasizing the importance of RDWT in texture and feature extraction. Without these features, the model

achieves an accuracy of 98.129 %, showcasing the contribution of GLCM in capturing texture and colour information for effective classification. In addition, consider the impact of excluding mean features, STD features, and colour features from MFEUsLNet. Here, without certain features, the model maintains lower performance, underscoring the adaptability and resilience of the proposed approach. Finally, the overall MFEUsLNet model achieves outstanding performance with an accuracy

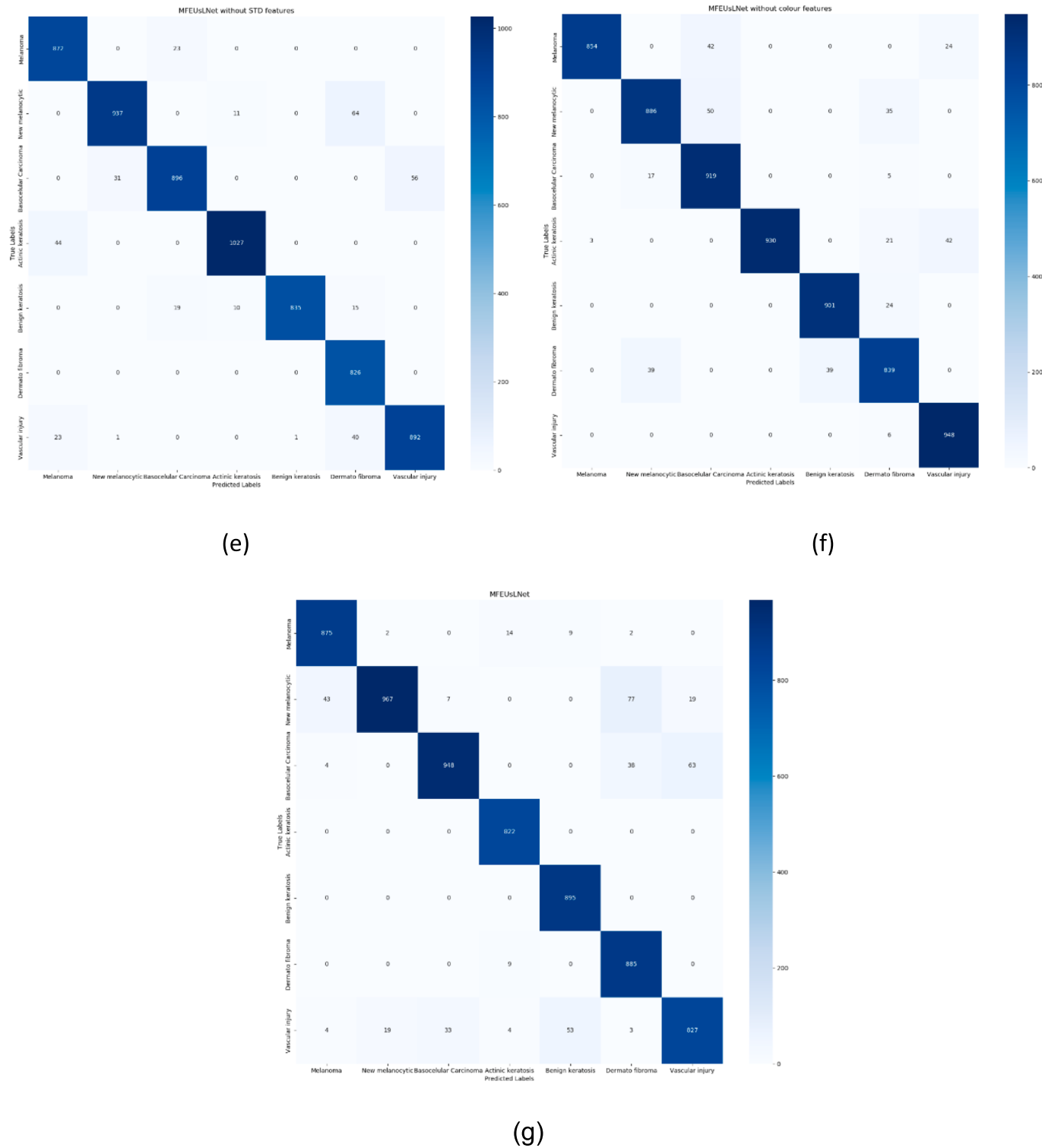


Fig. 12. (continued).

of 99.179 % and excels in all evaluated metrics. The percentages of improvement compared to the other scenarios are substantial, highlighting the comprehensive effectiveness of the integrated MFEUsLNet model for SCDC.

5. Conclusion

In this study, this work delved into the realm of skin cancer detection and classification, aiming to tackle the challenges identified in existing

literature while leveraging the strengths of machine learning and deep learning techniques. This research objectives encompassed the development of an effective skin cancer detection system, addressing limitations in previous methods, enhancing accuracy and interpretability, and evaluating proposed approach using the ISIC-2020 dataset. The cornerstone of our research is the MFEUsLNet system, a novel approach that combines the best practices in data preprocessing, lesion segmentation, feature extraction, and deep learning-based classification. The MFEUsLNet system not only builds upon the successes of previous

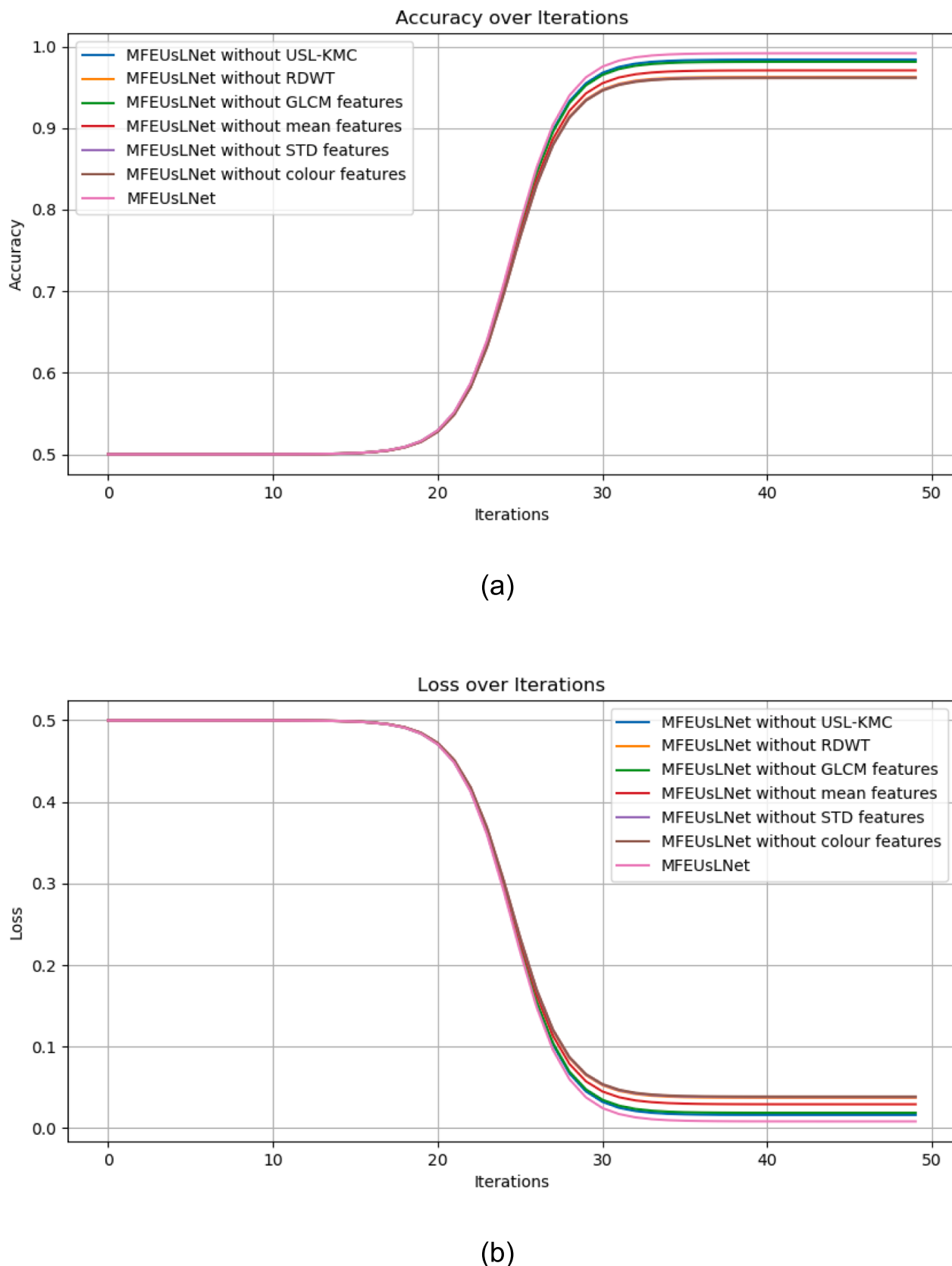


Fig. 13. Accuracy and loss graphs of ablation study. (a) Accuracy. (b) Loss.

methods but also addresses their limitations. This work has diligently worked towards mitigating the issues highlighted in the literature, particularly those concerning data quality, segmentation accuracy, interpretability, and the availability of comprehensive datasets. By incorporating a bilateral filter for noise removal and lesion enhancement, the USL-KMC method for precise lesion localization, and the GLCM and RDWT for feature extraction, our approach confronts these challenges head-on. The result is a system that not only boasts improved accuracy but also maintains transparency throughout the diagnostic process. The utilization of the ISIC-2020 dataset for rigorous evaluation is consistent with our hypothesis and research objectives. It serves as a robust benchmark, enabling us to assess the real-world applicability and performance of the MFEUsLNet system. This dataset, with its diverse and representative samples, ensures that our approach is put to the test against a wide spectrum of skin cancer cases. This research sets the stage for future developments, suggesting the potential extension of the approach to incorporate advanced deep learning techniques and optimization methods for the identification of a broader spectrum of diseases. Finally, the study contributes to the evolving landscape of skin cancer detection and classification, offering a promising pathway for enhanced diagnostic accuracy and efficiency.

Funding statement

No funding is received for this research work.

Declaration of competing interest

The authors declare that they have no known competing financial interests or personal relationships that could have appeared to influence the work reported in this paper.

Data availability

The data used to support the findings of this work are included in the article.

References

- [1] S. Haggemüller, et al., Skin cancer classification via convolutional neural networks: a systematic review of studies involving human experts, *Eur. J. Cancer* 156 (2021) 202–216.
- [2] M. Dildar, et al., Skin cancer detection: a review using deep learning techniques, *Int. J. Environ. Res. Public Health* 18 (10) (2021) 5479.
- [3] Rishu Garg, Saumil Maheshwari, Anupam Shukla, Decision support system for detection and classification of skin cancer using CNN, in: Innovations in Computational Intelligence and Computer Vision, Springer, Singapore, 2021, pp. 578–586.
- [4] Manikandan, Annamalai, M,Ponni Bala. (2023). Intracardiac Mass Detection and Classification Using Double Convolutional Neural Network Classifier. *Journal of Engineering Research*. 11(2A). 272-280. 10. 36909/jer.12237.
- [5] T. Saba, Computer vision for microscopic skin cancer diagnosis using handcrafted and non-handcrafted features, *Microscopy Res. Technique* 84 (6) (2021) 1272–1283.
- [6] M.A. Khan, et al., Multiclass skin lesion detection and classification via teledermatology, *IEEE J. Biomed. Health Inform.* 25 (12) (2021) 4267–4275.
- [7] M. Toğacıar, Z. Cömert, B. Ergen, Intelligent skin cancer detection applying an autoencoder, MobileNetV2, and spiking neural networks, *Chaos Solitons Fractals* 144 (2021) 110714.
- [8] S.M. Alizadeh, A. Mahloojifar, Automatic skin cancer detection in dermoscopy images by combining convolutional neural networks and texture features, *Int. J. Imaging Syst. Technol.* 31 (2) (2021) 695–707.
- [9] Manikandan Annamalai, Ponni Muthiah, An Early Prediction of Tumor in Heart by Cardiac Masses Classification in Echocardiogram Images Using Robust Back Propagation Neural Network Classifier, *Brazilian Archives of Biology and Technology* 65 (2022), <https://doi.org/10.1590/1678-4324-2022210316>.
- [10] S.K. Datta, et al., Soft attention improves skin cancer classification performance, in: *Interpretability of Machine Intelligence in Medical Image Computing and Topological Data Analysis and Its Applications for Medical Data*, Springer, Cham, 2021, pp. 13–23.
- [11] M. Balaji, S. Saravanan, M. Chandrasekar, G. Rajkumar, S. Kamalraj, Analysis of basic neural network types for automated skin cancer classification using the Firefly optimization method, *J. Ambient Intell. Humanized Comput.* 12 (7) (2021) 7181–7194.
- [12] G. Rajput, et al., An accurate and noninvasive skin cancer screening based on imaging technique, *Int. J. Imaging Syst. Technol.* 32 (1) (2022) 354–368.
- [13] A.K. Sharma, S. Tiwari, G. Aggarwal, N. Goenka, A. Kumar, P. Chakrabarti, M. Jasinski, Dermatologist-level classification of skin cancer using cascaded ensembling of convolutional neural networks and handcrafted features-based deep neural networks, *IEEE Access* 10 (2022) 17920–17932.
- [14] P. Thapar, M. Rakhra, G. Cazzato, M.S. Hossain, A novel hybrid deep learning approach for skin lesion segmentation and classification *Journal of Healthcare, Engineering* April 18 (2022) 2022.
- [15] V. Rotemberg, N. Kurtansky, B. Betz-Stablein, L. Caffery, E. Chousakos, N. Codella, M. Combalia, S. Dusza, P. Guitera, D. Gutman, A. Halpern, B. Helba, H. Kittler, K. Kose, S. Langer, K. Lioprys, J. Malvehy, S. Musthaq, J. Nanda, O. Reiter, G. Shih, A. Stratigos, P. Tschancl, J. Weber, P. Soyer, A patient-centric dataset of images and metadata for identifying melanomas using clinical context, *Sci. Data* 8 (2021) 34, <https://doi.org/10.1038/s41597-021-00815-z>.
- [16] M. Abdar, et al., Uncertainty quantification in skin cancer classification using three-way decision-based Bayesian deep learning, *Comput. Biol. Med.* 135 (2021) 104418.
- [17] A. Khamparia, et al., An internet of health things-driven deep learning framework for detection and classification of skin cancer using transfer learning, *Trans. Emerg. Telecommun. Technol.* 32 (7) (2021) e3963.
- [18] S. Ahmad, T. Ullah, I. Ahmad, A. Al-Sharabi, K. Ullah, R.A. Khan, S. Rasheed, I. Ullah, M. Uddin, M. Ali, A novel hybrid deep learning model for metastatic cancer detection, *Comput. Intell. Neurosci.* (2022).
- [19] S.P. Maniraj, P. Sardar Maran, A hybrid deep learning approach for skin cancer diagnosis using subband fusion of 3D wavelets, *J. Supercomput.* (2022) 1–16.
- [20] M. Nawaz, et al., Skin cancer detection from dermoscopic images using deep learning and fuzzy k-means clustering, *Microsc. Res. Tech.* 85 (1) (2022) 339–351.
- [21] V.S.S.P. Raju Gottumukkala, N. Kumaran, V. Chandra Sekhar, BLSNet: Skin lesion detection and classification using broad learning system with incremental learning algorithm, *Expert Systems* 39 (9) (2022) e12938.
- [22] P. Bharat Siva Varma, et al., SLDCNet: skin lesion detection and classification using full-resolution convolutional network-based deep learning CNN with transfer learning, *Expert. Syst.* (2022) e12944.
- [23] H.C. Reis, et al., InSiNet: a deep convolutional approach to skin cancer detection and segmentation, *Med. Biol. Eng. Comput.* 60 (3) (2022) 643–662.
- [24] K.S. Kumar, et al., FSPBO-DQN: SeGAN-based segmentation and fractional student psychology optimization enabled deep Q network for skin cancer detection in IoT applications, *Artif. Intell. Med.* 129 (2022) 102299.
- [25] U. Bhimavarapu, G. Battineni, Skin lesion analysis for melanoma detection using the novel deep learning model fuzzy GC-SCNN, *Healthcare* 10 (5) (2022). MDPI.
- [26] Kolli, Srinivas & V., Praveen & John, Ashok & Manikandan, A.. (2023). Internet of Things for Pervasive and Personalized Healthcare: Architecture, Technologies, Components, Applications, and Prototype Development. 10.4018/978-1-6684-8913-0.ch008.
- [27] A.M. Teodoro, et al., A skin cancer classification approach using GAN and RoI-based attention mechanisms, *J. Signal Process. Syst.* (2022) 1–14.
- [28] M.D. Khan, et al., Skin cancer detection from low-resolution images using transfer learning, in: *Intelligent Sustainable Systems*, Springer, Singapore, 2022, pp. 317–334.
- [29] F. Afza, et al., Multiclass skin lesion classification using hybrid deep feature selection and an extreme learning machine, *Sensors* 22 (3) (2022) 799.
- [30] R. Ali, A. Manikandan, J. Xu, A Novel framework of Adaptive fuzzy-GLCM Segmentation and Fuzzy with Capsules Network (F-CapsNet) Classification, *Neural Comput. & Applic.* (2023), <https://doi.org/10.1007/s00521-023-08666-y>.
- [31] Pronab Ghosh, Sami Azam, Ryana Quadir, Asif Karim, F.M. Shamrat, Shahog Kumar Bhowmik, Mirjam Jonkman, Khan Md Hasib, Kawsar Ahmed, SkinNet-16: a deep learning approach to identify benign and malignant skin lesions, *Front. Oncol.* 12 (2022) 931141.
- [32] A. Javaid, M. Sadig, F. Akram, Skin Cancer Classification Using Image Processing and Machine Learning, in: 2021 International Bhurban Conference on Applied Sciences and Technologies (IBCAST), Islamabad, Pakistan, 2021, pp. 439–444. doi: 10.1109/IBCAST51254.2021.9393198.
- [33] A.S. Qureshi, T. Roos, Transfer learning with ensembles of deep neural networks for skin cancer detection in imbalanced data sets, *Neural Process. Lett.* 55 (2023) 4461–4479, <https://doi.org/10.1007/s11063-022-11049-4>.
- [34] M.A. Araaf, K. Nugroho, Comprehensive analysis and classification of skin diseases based on image texture features using K-nearest neighbors algorithm, *J. Comput. Theories Appl.* 1 (1) (2023) 31–40.
- [35] F. Mustofa, A.N. Safriandono, A.R. Muslih, Dataset and feature analysis for Diabetes Mellitus classification using random forest, *J. Comput. Theories Appl.* 1 (1) (2023) 41–48.